Method to obtain nonuniformity information from field emission behavior

Fernando F. Dall'Agnol, Alexandre C. de Paulo, Pablo Paredez, Daniel den Engelsen, Thebano E. A. Santos, and Victor P. Mammana

Method to obtain nonuniformity information from field emission behavior

Fernando F. Dall'Agnol,[a] Alexandre C. de Paulo, Pablo Paredez, Daniel den Engelsen,
Thebano E. A. Santos, and Victor P. Mammana
*Centro de Tecnologia da Informação Renato Archer (CTI), Rod Dom Pedro I, km 143.6, Campinas,
13069-901 São Paulo, Brazil*

This article describes the characterization of field emission from a planar cathode to a spherical anode with the approach curve method (ACM). In such a diode configuration the electric field strength at the cathode surface is nonuniform. This nonuniformity gives an extra degree of freedom and it allows the interpretation of the current-voltage and voltage-distance ($V \times d$) curves in terms of nonuniformity. The authors apply the ACM to Cu emitters to explain the nonlinearity of the $V \times d$ curve in ACM measurements. This analysis provides a good insight into field emission phenomena, supporting a method for nonuniformity characterization based on field emission behavior. © *2010 American Vacuum Society.* [DOI: 10.1116/1.3327928]

I. INTRODUCTION

The publication of the pioneer work of Spindt[1] raised the interest in field emitters considerably and many publications appeared in the past decades on the preparation,[2,3] characterization,[4,5] and application of field emitters.[6] In this study, we focus on the characterization of field emission (FE) measured in a diode, which is placed in a high-vacuum chamber. Usually, field emission is measured with a flat cathode and anode; since such a diode yields a uniform field, it enables a direct conversion of the applied voltage difference V into the field strength E through the equation $E = V/d$, where d is the distance between the anode and the cathode. Usually, d is defined accurately using spacers between the anode and the cathode. Spacers may induce flashovers and limit the application of high field strengths. Mammana *et al.*[5] reviewed this problem and proposed the approach curve method (ACM) to avoid the use of spacers and to allow an accurate determination of the diode distance d if the anode and cathode planes are parallel. The ACM was also used by Gröning *et al.*[7] to accurately determine the turn on field at a low emission current. Figure 1 is a simulation to illustrate the ACM method. In Fig. 1(a) the cathode-anode distance is varied step by step in such a way that the anode is moved perpendicularly toward or from the cathode in an accurate way. At each step of d a complete $I \times V$ curve is measured and many $I \times V$ curves are obtained. At a given current I_C, all values V_n, defined at the intersection points of the individual $I \times V$ curves and the line $I = I_C$, are generated and plotted in a separate $V \times d$ diagram, as shown in Fig. 1(b). As can be seen, this yields a straight line. The point where this line intersects with the horizontal at $V = 0$ determines the correction to get the true diode distance d_n for each step. In this simulation, the correction in d_n is -25 μm, so d_1 is actually 35 μm, not 60 μm as first estimated.

In FE studies, parallel plane electrodes are preferred because it is easier to describe the macroscopic field. Neverthe-less, the deviation from parallelism between the electrodes will increase the inaccuracy at very small cathode-anode gaps, and fringe effect may cause the mathematical treatment to be difficult, as analyzed in Ref. 5. A principal way in eliminating the aforementioned difficulties is using a spherical anode. Parallelism is, in this case, not an issue, whereas the electric field becomes nonuniform in a known and well-defined way. In other words, the electric field distribution in a sphere-plane diode is simpler than the field in plane electrodes with a fringe field.

The field distribution of a sphere-plane diode, in which the sphere can be either anode or cathode, is treated in many studies on field emission and some textbooks on electrostatics as well.[8–10] Cloete and van der Merwe[11] and Butler[12] used the well-known algorithm of image charges to obtain the field and potential distributions. Unfortunately, these authors did not provide the final expressions for the field and potential distributions. Although this straightforward algorithm leads to a series expansion, which needs many terms in the case of a small gap compared to the radius of the sphere, the computation time to calculate the field is still negligible in the worst cases we have considered. An algorithm to calculate the field enhancement of a "floating sphere at emitter-plane potential" between two flat electrodes was published by Miller[13] and reviewed recently by Forbes *et al.*[14] The latter authors also calculated the field distribution of this configuration, which has a different boundary condition than the problem we are interested in. They solved the Laplace equation for this configuration by means of a finite element method. For a similar configuration—a hemisphere on a post—the field enhancement was also computed by Forbes and it has been treated again recently by le Fèbre *et al.*[15] This configuration has also different boundary conditions than our problem; therefore, we shall not make use of their results. So, the first objective of our study is to present the potential and electric field distributions of a diode consisting of a flat cathode and a spherical anode in a convenient analytical way because neither the literature on the method of images nor

---

[a]Electronic addresses: fernando.dallagnol@cti.gov.br and ffdallagnol@hotmail.com
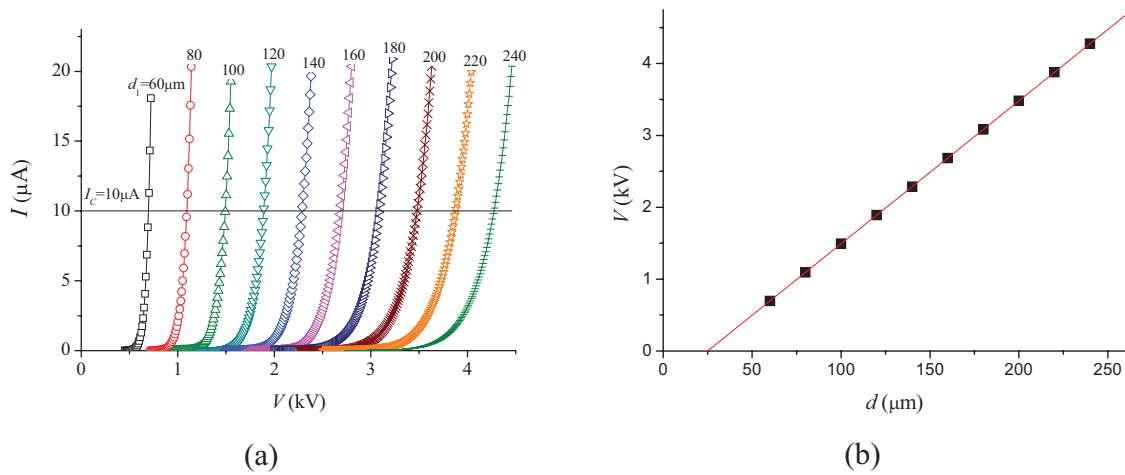
FIG. 1. (Color online) Illustration of the approach curve method. In (a) a constant current I_C intercepts the curves of the simulated $I \times V$ data. (b) Intersections are points in a $V \times d$ diagram forming a straight line that should intercept the origin; the shift in the d-axis is used to calibrate the distances d_n.

the literature on spherical shaped protrusion provides complete expressions for the field and potential distribution.

The second or main objective is to simulate the effect of a nonuniform distribution of emitters in a sphere-plane electrodes system using the approach curve method. We will explain the characteristics of the field emission according to this method including the difficulties in getting reproducibility.

The outline of this article is as follows. In Sec. II we derive the potential and the electric field distributions of the planar-spherical diode. In Sec. III we show some measurements performed with a Cu flat cathode and an anomaly in the $V \times d$ curve. In Sec. IV we explain this anomaly due to the nonuniformity of the emitters. The experimental setup and measurements are presented before the models because the range of the parameters will be based on the experimental dimensions. This allows us to focus merely on the parameters referring to our model. In Sec. V we present the conclusions, future works, and possible applications in microscopy. Finally, in the Appendix we present several other models that are physically reasonable and would also explain the observed anomaly in $V \times d$. We show that these models do not quantitatively account for the phenomenon observed.

II. SPHERE-PLANE ELECTRODES

In this section we derive the potential and field distributions of a diode consisting of a flat conductive cathode and spherical conductive anode. Figure 2 shows the diode arrangement and the cylindrical coordinates r and z (the azimuth is not indicated).

As mentioned before, a sphere-plane electrode arrangement presents some advantages compared to parallel plane configurations mainly because it has no fringe effects and no alignment problem. The field strength E is not constant on the surface of the cathode, but rather depends on the distance from the symmetry axis. E is obtained by the image charge method with boundary conditions of the potential being V at the anode and zero potential at the cathode surface.

To solve the potential for this system using image charges, we start considering an isolated sphere with charge q_0, which generates the potential V at the surface. Then, q_0 can be expressed in terms of its resulting potential V as

$$q_0 = \frac{aV}{k}, \tag{1}$$

where $k = 9 \times 10^9$ Vm/C is the electrostatic constant. In the presence of the plane at $z=0$, charge q_0 generates an image of the same magnitude and opposite sign $-q_0$ at position $-z_0$. The image charge $-q_0$ also generates an image in the sphere with position and magnitude given by

$$z_1 = z_0 - \frac{a^2}{2z_0}, \tag{2}$$

$$q_1 = \frac{a}{2z_0} q_0. \tag{3}$$

This situation is depicted in Fig. 3(a). The image charge q_1, in turn, generates $-q_1$ at the plane, which generates q_2 in the sphere and so on. Figure 3(b) represents the final charge
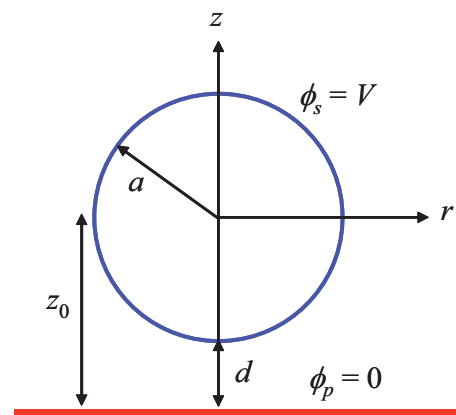

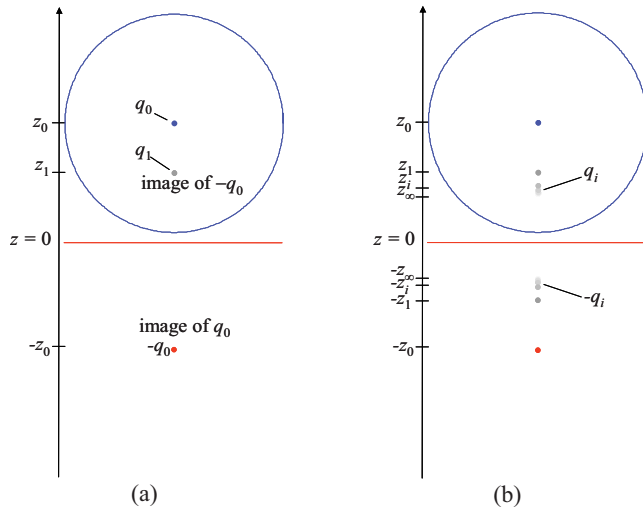FIG. 2. (Color online) Sphere-plane electrodes in a cylindrical coordinate system for field emission studies.

FIG. 3. (Color online) Composition of the two systems of image points. (a) Representation of the first two images generated by the real charge and (b) the final distribution of image charges.

distribution. The position and magnitude of the ith image charge are given by the recurrent relations,

$$z_i = z_0 - \frac{a^2}{z_0 + z_{i-1}}, \quad (4)$$

$$q_i = \frac{a}{z_0 + z_{i-1}} q_{i-1}. \quad (5)$$

A similar derivation of image charges in a system of two spheres was done in Refs. 8–12 and will not be repeated here. It is convenient to define a normalized charge $\xi_i = q_i/q_0$, which will be used to present the solution more concisely. Dividing Eq. (5) by q_0, we get

$$\xi_i = \frac{a}{z_0 + z_{i-1}} \xi_{i-1}, \quad (6)$$

with $\xi_0 = 1$. For $i \to \infty$, parameters $\xi_i \to 0$ and $z_i \to z_\infty$ (constant). The potential due to a charge of index i in the sphere and its image in the plane are given by

$$\phi_i = k \left(\frac{q_i}{[(z - z_i)^2 + r^2]^{1/2}} - \frac{q_i}{[(z + z_i)^2 + r^2]^{1/2}} \right). \quad (7)$$

The potential due to all charges is completely determined by summing ϕ_i, and using Eqs. (1) and (5) in Eq. (7) results in

$$\phi(r,z) = aV \sum_{i=0}^{\infty} \frac{\xi_i}{[(z - z_i)^2 + r^2]^{1/2}} - \frac{\xi_i}{[(z + z_i)^2 + r^2]^{1/2}}. \quad (8)$$

The macroscopic electric field can be obtained from $\mathbf{E}(r,z) = -\nabla \phi$, resulting in

$$E_r(r,z) = aVr \sum_{i=0}^{\infty} \frac{\xi_i}{[(z - z_i)^2 + r^2]^{3/2}} - \frac{\xi_i}{[(z + z_i)^2 + r^2]^{3/2}}, \quad (9)$$
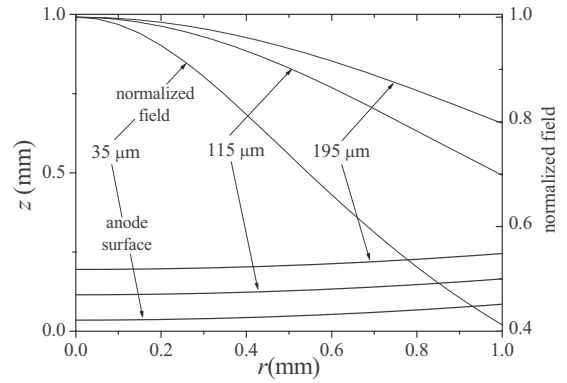
FIG. 4. Normalized field distribution at the sample surface for anode-cathode distances of 35, 115, and 195 μm in a cylindrical (r,z) coordinate system for $a=1$ cm.

$$E_z(r,z) = aV \sum_{i=0}^{\infty} \frac{\xi_i(z - z_i)}{[(z - z_i)^2 + r^2]^{3/2}} - \frac{\xi_i(z + z_i)}{[(z + z_i)^2 + r^2]^{3/2}}, \quad (10)$$

where E_r and E_z are the components of the field in the r and z directions, respectively. The modulus of the field, $E(r)$, at the conducting plane is obtained making $z=0$ in Eqs. (9) and (10). Then, E_r vanishes and only E_z contributes to E, resulting in

$$E(r) = aV \sum_{i=0}^{\infty} \frac{2\xi_i z_i}{(r^2 + z_i^2)^{3/2}}. \quad (11)$$

The convergence of the sum in Eq. (11) depends on the r coordinate and on the sphere-plane distance d. At $r=0$ and z_0/a as small as 1.01, the convergence to 99.9% is obtained with 55 terms in the sum. We find slightly different accuracies when comparing the z_∞ with z_i, as mentioned by Buttler,[12] viz., 2 parts in 10^8 for $i=20$ and $z_0/a=1.1$ and 5 parts in 10^7 for $i=170$ and $z_0/a=1.001$. Figure 4 shows that E has a Gaussian-type profile as a function of r. The width of the normalized field distribution becomes larger upon increasing the cathode-anode distance, favoring emission farther from the axis.

Once $E(r)$ is given, the current density can be evaluated according to the Fowler–Nordheim (FN) formula,[7,16]

$$j_{\beta\omega} = A \frac{\beta^2}{\omega} E^2 \exp\left(-B \frac{\omega^{3/2}}{\beta E} \right), \quad (12)$$

where $A = 1.54 \times 10^{-6}$ A eV V^{-2}, $B = 6.83 \times 10^9$ eV$^{-3/2}$ V m^{-1}, β is the field amplifying factor, and ω is the work function in eV. The overall current is obtained by integrating j over an effective area; however, the effective area depends on the particular model to be discussed in Sec. V.

III. MEASUREMENTS IN PURE COPPER

Field emission measurements in high-vacuum condition ($<10^{-5}$ Pa) were performed by applying a voltage ramp between a spherical anode with radius of $a=1.0$ cm and a 1.5×1.5 cm^2 flat cathode of pure copper. The cathode
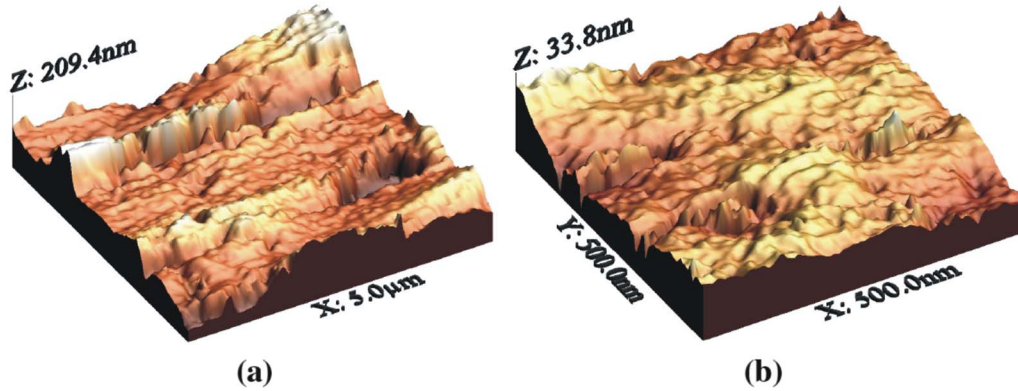
FIG. 5. (Color online) Atomic force microscopy of the Cu sample for (a) 5×5 μm^2 and (b) 0.5×0.5 μm^2.

sample is flat in a macroscopic sense, but rough on a micro-metric scale, as shown in Figs. 5(a) and 5(b), being the atomic force microscopy (AFM) pictures of our sample. These figures were obtained with an AFM-Autoprobe CP (Park Scientific Instruments). Note in Fig. 5(a) that the maximum height of the protrusions is about 150 nm. Figure 5(b) shows the Cu surface at an amplification 100 times higher. From these figures, we conclude that our sample has a distribution of protrusions between ~20 and 150 nm.

$I\times V$ curves are measured for nine values of d varying from 35 to 195 μm in accurate steps of 20 μm and are shown in Fig. 6. It can be noticed from this figure that the curves are getting closer to each other at greater d. This is already an indication that the $V\times d$ curve is concave down, as will be shown hereafter. The dotted horizontal line represents a constant current of $I_C=10$ μA chosen arbitrarily. This line intercepts all $I\times V$ curves. The intersections are used to plot a $V\times d$ curve, as shown in Fig. 7. The full line is the fitting with a parabola with quadratic coefficient $Q= -(53\pm5)\times10^9$ V/m². The straight dashed line in this figure shows the departure from linearity. One is tempted to assume that in sphere-plane electrodes this $V\times d$ nonlinearity may be only an effect of the roundness of the anode. Indeed, equations for a uniform emission in sphere-plane electrodes predict a concave down curve when $d\ll a$. Note that this is the case in these measurements. However, in the Appendix we

will show that the concaveness due to the geometry of the electrodes is negligible at our experimental conditions.

In Fig. 8 we present the FN plots of the measurements, as is traditionally done to indicate nonlinear behavior and to show what part of the curve is used for fitting parameters. Our FN plots at various values of the anode-cathode distance do not present an evident deviation from straight lines. Nicolaescu[17] demonstrated that nonuniform emitters may cause nonlinear behavior in the FN plot. Since the nonuniform carbon nanotube (CNT) samples of Gröning *et al.* yield linear FN plots, it may be concluded that the FN plot is not a good criterion to decide on the uniformity of field emission samples. We think that the $V\times d$ curves present a better criterion: the negative concaveness observed in Fig. 7 is the main experimental feature we aim to explain in terms of nonuniform emitter model to be presented in Sec. IV.

We stress that our experiments are shown before the models to restrict the parameters of the simulation such as, anode-cathode distance range, current and voltage ranges, field amplifying factor, work function, sphere radius, etc.

IV. NONUNIFORM SITE EMITTERS MODELS

In this section we simulate the field emission for a nonuniform distribution of emitters. We start analyzing the simplest model with one emitter and then with two emitters.
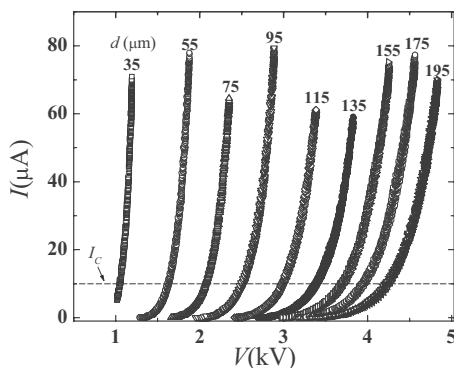

FIG. 6. $I\times V$ curves for nine anode-cathode distances. Intersections of the curves with I_C are points (d_n, V_n) to plot a $V\times d$ graphic.
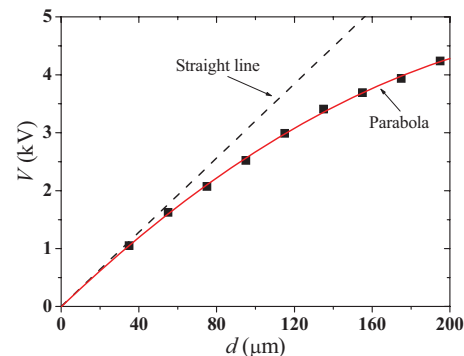

FIG. 7. (Color online) Experimental $V\times d$ curve for Cu fitted with a parabola concave down. The straight line is shown to reveal the deviation from linearity.
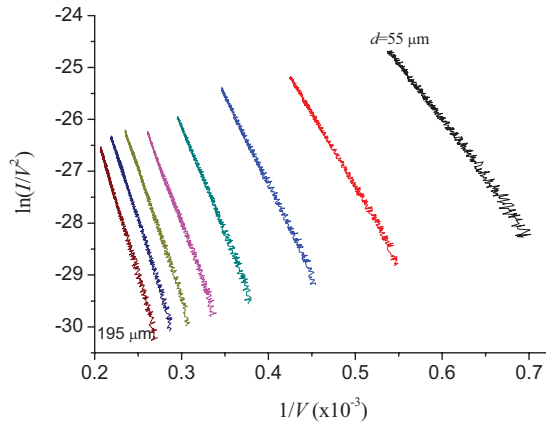
FIG. 8. (Color online) FN plots of the measurements appear quite straight despite the nonuniform distribution of the emitters and of the field.
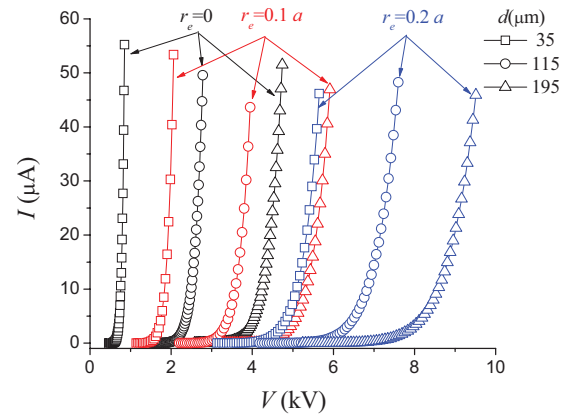

FIG. 9. (Color online) $I \times V|_{sim1}$ simulation for a single emitter for $d=35$, 115, and 195 μm and for $r_e=0$, $0.1a$, and $0.2a$.

With two emitters we can adequately explain the effect of nonuniformity on the $V \times d$ characteristics. Then, we extend the idea to a more realistic case with a random distribution of emitters and its consequent FE characteristics.

A. Model of one emitter

For this model, we investigate the effect of the displacement of the radial coordinate r_e of one emitter with respect to the symmetry axis ($r=0$). The current is assumed to be $I = Sj_{\beta\omega}(r_e)$, where S is the effective area of the emitter and the FN parameters β and ω are defined in Eq. (12). We first need to determine reasonable values for S and β of a single emitter in order to enable a sensible comparison with the experimental data. We fit S and β to the $I \times V$ experimental curves using $r_e=0$ and the work function of copper $\omega_{Cu} \approx 4.7$ eV.[18] Typically, we obtain $S=1$ μm^2 and $\beta=250$. We will assume these values as constants for the simulations. The effective emission area obtained is reasonable for this sample. Note in Fig. 5(a) that the lateral size of the irregularities is about 1 μm. We expect one of these protrusions to be higher than the average, causing most of the emission. Figure 5(b) shows that there are also protrusions as small as 20 nm: these are not considered in this simple one emitter model. The $I \times V|_{sim1}$ and $V \times d|_{sim1}$ diagrams, simulated with these parameters, are shown in Figs. 9 and 10, respectively. At a fixed d, the $I \times V|_{sim1}$ curves have higher onset voltages than the experimental curves and the $V(d)$-curve does not intercept the origin either. These features may be explained by realizing that the actual distance between the emitter and the anode tends to be constant and slightly different from 0 at $d \rightarrow 0$, except for the rare particular case $r_e=0$. Furthermore, the $V(d)$ concaveness is positive, i.e., the quadratic coefficient Q is >0 (not shown), instead of negative. So, one emitter fails completely to predict the negative concaveness in $V(d)$. This can be explained by realizing that for $d \rightarrow 0$, the electric field is much stronger close to the z-axes than at r_e. Then, for sufficiently small d, bad emitters close to the z-axes will start emitting stronger than a good emitter at r_e and this is excluded in our one emitter model.

B. Model with two emitters

Following the idea of the previous section, we now consider one bad emitter at the z-axis ($r=0$) and one good emitter at r_{e2}. We suppose ω and S to be constant with the same values as in Sec. IV A. We assume a bad emitter $\beta_{bad}=125$ at coordinate r_{e1} and a good emitter $\beta_{good}=250$ at r_{e2}. The $I \times V|_{sim2}$ curves for $r_{e2}=0.14a$ are shown in Fig. 11. Note that the distances between the curves are smaller for higher voltages, which was also observed in the experimental curves in Fig. 6. The corresponding $V \times d|_{sim2}$ for $I_C=10$ μA is shown in Fig. 12 together with two other curves for $r_{e2}=0.1a$ and $0.2a$. The quadratic coefficient Q is indicated in this figure, obtained from the fitting with a parabola (full lines). Q is very sensitive to variations in r_{e2}. In Fig. 13 we plot Q as a function of r_{e2} to show that it presents a minimum, going from positive to negative to positive concaveness again, overlapping the experimental value of $-(5.3 \pm 0.5) \times 10^{10}$ V/m^2.

Notice that the intersections of the parabolas with the d-axis in Fig. 12 do not intercept the $V=0$ axis at the origin. So the ACM of a nonuniform sample may not provide a good correction to the electrode's distances if their initial separa-
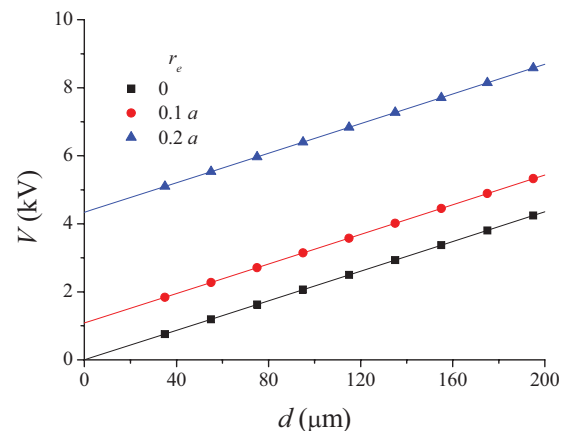

FIG. 10. (Color online) ACM simulation for a single emitter at coordinates $r_e=0$, $0.1a$, and $0.2a$.
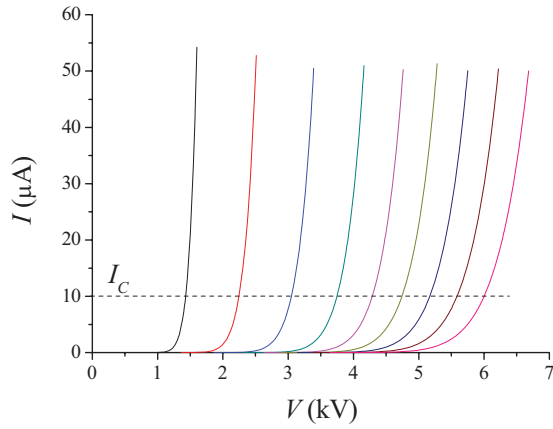
FIG. 11. (Color online) $I \times V|_{\text{sim2}}$ for $r_{e2}=0.14a$. The distances between the curves are smaller for higher voltages.

FIG. 13. $Q \times r_{e2}$ diagram showing the behavior of the concaveness in $V \times d$, starting from the slightly positive, becoming strongly negative reaching a minimum value and then slightly positive again. The dashed line shows $Q=0$ to guide the eye.

tion is not sufficiently small. Take, as an example, the parabola for $r_{e2}=0.10a$ intercepting d-axes at -20 μm: an attempt to calibrate the distances would make them $+20$ μm greater than their actual values from 35 to 195 μm. So, nonuniform samples may limit the application of the ACM. A way to solve this problem is to make several ACM measurements displacing the anode laterally in order to infer r_{e2}. This will be discussed in Sec. IV C when we point out a possible application of the ACM in microscopy.

Two emitters can easily reproduce the concaveness observed using reasonable values for the field enhancement parameter. It is worth to mention that several other models were tried to explain the $V \times d$ concaveness. These models are physically plausible, but they failed in predicting the concaveness quantitatively, unless using unreasonable values for the parameters in the simulations. This is why we believe that nonuniformity is the best model that explains the concaveness in $V(d)$. The other models that we investigated are presented in the Appendix.

With this model, the concaveness can be obtained with a wide range of $\beta_{\text{bad}}/\beta_{\text{good}}$ and of r_{e2}. Furthermore, the emitter we supposed to be fixed at $r=0$ may also be a little bit off
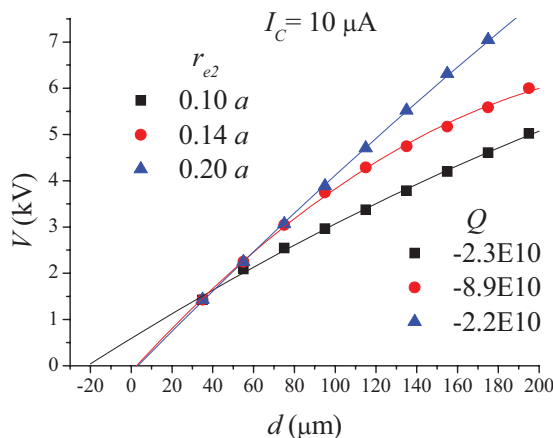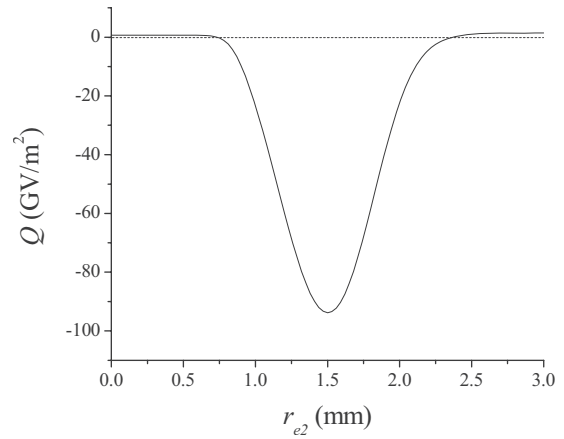
axis, and yet, the concaveness observed will be reproduced. More than two emitters can also represent the experimental concaveness, as will be shown in Sec. IV C.

C. Random distribution of emitters

Now we consider the situation representing a more realistic sample where emitters are randomly distributed. We analyze Q as the anode is moved laterally in straight lines above the cathode. We consider two types of emitters distributed, as represented in Fig. 14, for a 4 cm^2 sample. Dots are bad emitters with $\beta_1=125$ and triangles are good emitters with $\beta_2=250$. We need to make β_1 much more numerous than β_2 to simulate the presence of a bad emitter close to the symmetry axis. This is necessary to account for the emission close to the z-axis at small d, as discussed in Sec. IV A. Furthermore, in a real sample the number of very good emitters is small. Here, we assume that the number of bad emitters is ten times larger than the number of good emitters. In Fig. 14 the lines with labels (1)–(3) show the paths of the anode. At every 0.1 mm, a complete ACM measurement is

FIG. 12. (Color online) Concavity for three r_{e2} values. The extrapolation of the curves does not contain the origin.
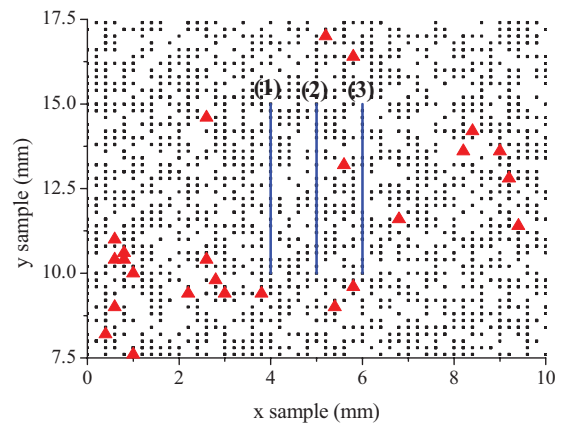

FIG. 14. (Color online) Representation of a fragment of the sample indicating good emitters (triangles), bad emitters (dots), and three paths where the sample is scanned by the anode.
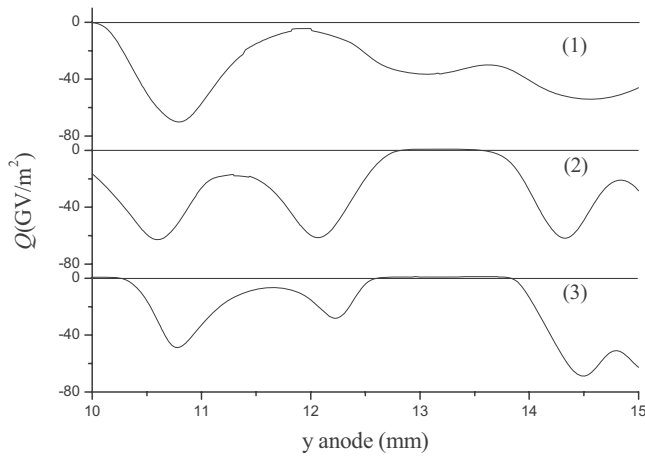
FIG. 15. Quadratic coefficient as a function of the anode position for paths (1)–(3). These scans may provide the positions of the emitters. The concavity of $V(d)$ for values of $Q < 5$ GV/m^2 is difficult to be noticed.

FIG. 16. (Color online) Dispersion in $I \times V$ curves, taken at every 0.2 mm in path (3), showing the nonreproducibility in a nonuniform sample.

simulated and Q is obtained as a function of the y coordinate shown in Fig. 15 for these three lines. When Q is smaller than 5 GV/m^2, the concavity of $V(d)$ is difficult to be noticed. Indeed, $V(d)$ does not always present a noticeable concavity. We assert that about 70% of the measurements present a noticeable concavity and this model is successful in explaining this proportion. The average spatial distribution between good emitters of 1 mm (see Fig. 14) was chosen in order to approximate the Q observed. Other authors presented images, showing the same approximate separation among the protrusions.[2,19] From the AFM pictures in Fig. 5, it is difficult to derive an average distance between good emitters because besides height, the radius of the tip is also important.

We are able to construct a $Q \times y$ diagram using the random positions of the emitters. The other way around is more difficult, i. e., find the positions of the emitters by mapping Q from $I \times V$ curves. In a real sample there are impurities, β has a distribution, emission usually changes the surface, etc., to mention a few complications. In this work, we show the effect of nonuniformity, but the way back to find the distribution from its FE effects is still under study. This may provide applications in FE microscopy since emitters are hallmarks of the surface.

Nonuniformity is one of the big issues of field emitters and this property has been investigated by many scientists. From the wealth of literature on this subject, we shall refer to an important study in 2000 published by Gröning *et al.*[7]

Gröning *et al.* found an exponential distribution of the enhancement factor β for plasma enhanced CVD (PECVD) grown CNTs. This implies that with increasing field strength, the number of CNTs that starts emission increases. When we also assume that the number of emitters increases with the field strength for our copper cathode, we expect that the ACM would generate smaller absolute values for the curvature Q of the $V(d)$-curves at different current because the emission site density will change as a function of current (or field strength) since the emission becomes more uniform. In
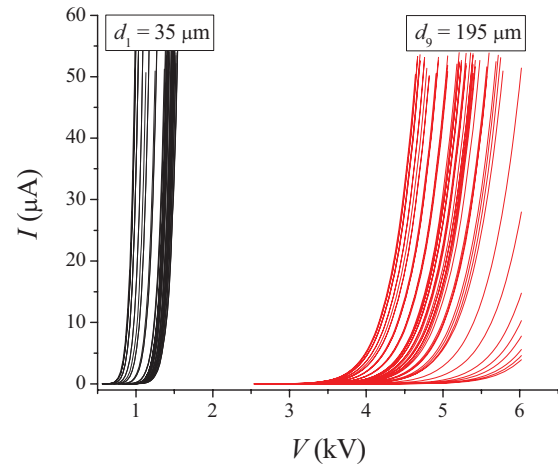
fact, we find a small increase in Q of the experimental $V(d)$-curves by increasing the current. This result indicates that the copper sample behaves quite different from the CNT sample made by Gröning *et al.*, i.e., the number of emission sites of the copper cathode does not change significantly by increasing the field strength.

Another important feature in a nonuniform sample is the dispersion in $I \times V$ curves, as shown in Fig. 16 for $d_1 = 35$ μm and $d_9 = 195$ μm. These curves are taken at every 0.2 mm in path (3). Note that a sample may present nonreproducibility if displaced between one measurement and the other due to the sensible dependence of the $I \times V$ characteristics on the anode position. This shows how difficult it is to compare measurements between samples, which are macroscopically identical. The nonuniformity will cause the measurements to become "nonreproducible."

V. CONCLUSION

In this article, we have described an extension of the ACM from a planar diode to a diode consisting of a planar cathode and a spherical anode. We have presented analytical formulas for the potential and field distributions of the electric field or such a diode configuration. The abnormal behavior of the ACM of a sample of Cu emitters could be explained in terms of nonuniformity of the emission. This result indicates that planar-spherical diodes are powerful tools to investigate field emission since one obtains information on the nonuniformity. In a nonuniform distribution of emitters, the ACM may not give a correct calibration of the anode distance. We showed that the nonuniformity may cause an apparent nonreproducibility because of the sensible dependence of the $I \times V$ characteristics on the position of the anode. We have also indicated that scanning the quadratic coefficient of the $V(d)$ overall the sample provides a sensitive map of its nonuniformity. Possibilities for a new way of FE microscopy need to be explored further.

APPENDIX: OTHER MODELS TESTED

Here we present some models analyzed and rejected since they could not predict quantitatively the concave down in $V(d)$. These models need to be discussed because they are physically plausible. We studied them to be more confident that the nonuniformity of the sample is the main reason of negative $V(d)$ concaveness.

1. Effect of the sphere-plane geometry

As we have discussed in Sec. IV, the geometry of the electrodes causes a negative concaveness of the $V \times d$ curve if the emitters are identical and homogeneously distributed. In this case, the overall current can be expressed as the integral of the current density j over the area of the sample,

$$I = 2\pi S_e \int_0^\infty r j_{\beta\omega}(r)dr, \tag{A1}$$

where S_e is a dimensionless parameters so that $2\pi S_e r dr$ is the effective area of emission in a ring of radius r and width dr. Within the range of 35 μm $\leq d \leq$ 195 μm, the upper limit of $r = a$ in Eq. (A1) is more than enough to compute I. Using $\beta = 250$ and $\omega_{Cu} = 4.7$ eV, $S_e = 6.8 \times 10^{-7}$ and $I_C = 10$ μA, the simulations of the emission predicts the quadratic coefficient $Q_{theor} = -6.55 \times 10^9$ V/m^2, which is approximately eight times smaller than the value observed $Q_{obs} = -(53 \pm 5) \times 10^9$ V/m^2.

2. Electrons trajectories

Electrons departing from the cathode do not always reach the anode. It is tempting to assume that more electrons are collected when the anode is moving away from the cathode. In this case, the voltage at the anode does not need to be increased proportionally to the distance in order to keep the current constant. Less increment in the voltage would be sufficient to keep the current constant. Then, this would be a physical reason for the negative Q observed. Figure 17 shows electron trajectories starting at fixed emitters. The
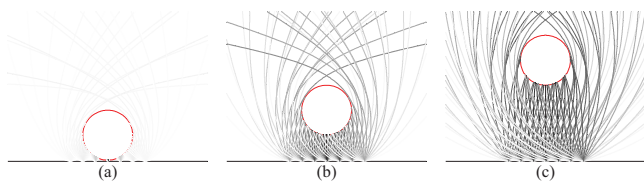

FIG. 17. (Color online) Trajectories of electrons for three anode distances. The farther the anode, the fewer electrons are collected due to the angular distribution.

darker the line, the stronger the emission represented in that trajectory. This figure shows trajectories of electrons departing from different radial coordinates with an angular distribution.[20] Contrary to what was expected, the farther the anode is moved from the cathode, the fewer electrons are collected, which contributes for a positive Q. Furthermore, the displacement of the anode in these measurements is about a hundred times smaller than the radius of the sphere, while these simulations shows a noticeable variation in the number of electrons collected only for displacements up to $3a$. So we can assert that variation in the electrons collected due to the anode displacement is utterly negligible. This does not contribute for the value of Q in this experiment.

3. Resistance and space charge effects

Another obvious possibility to explain the observed negative value Q would be the electrical resistance of the sample. The equation for a constant current I_C for a uniform sample is

$$I_C = k_1 \int_0^\infty E_R^2 \exp\left(-\frac{k_2}{E_R}\right) r dr, \tag{A2}$$

where $k_1 = 2\pi A S_e \beta^2 / \phi = 8.75 \times 10^{-8}$ V/m^2 and $k_2 = B\phi^{3/2}/\beta = 2.78 \times 10^8$ V/m. Here, k_1 and k_2 were introduced to simplify (A2). Now, the field is given by

$$E_R = (V - I_C R) \sum_{i=0}^\infty \frac{2\xi_i z_i}{(r^2 + z_i^2)^{3/2}}. \tag{A3}$$

Note that the term $I_C R$ is more significant when V is low, i.e., for small d. As d increases (V to obtain I_C also increases), the term $I_C R$ has smaller influence on the effective voltage. So the applied voltage does not have to compensate this term anymore and the step in V could be expected to increase in a proportion smaller than d, causing $V(d)$ to be concave down. This model fails in two aspects: first, the value of R must be of the order of 10 MΩ to influence the applied voltage, which is too high for copper; second, the $I \times V$ curves becomes tilted for high voltages, which is not observed experimentally. Figure 18 shows the resistance effect for $R = 100$ MΩ.

Space charge can also limit the current for small d by shielding the voltage drop between anode and cathode, so the applied voltage has to be higher to generate a current I_C in a similar way that the resistance does. As d increases, more emitters contribute, the current density becomes smaller, and the space charge effect vanishes. Less increment in the voltage is needed to achieve I_C, causing the concave down in $V(d)$. This would be also physically plausible. Nevertheless, fitting any of the curves with Eq. (12), we find an effective area S close to 1 μm^2. The higher current in our measurements is 80 μA. So, even considering only one emitter as in Sec. VA, the highest current density we have is of the order of 10^4 A/cm^2, which is much below the current density required for space charge, i.e., 10^6–10^7 A/cm^2 (Refs. 21–23).
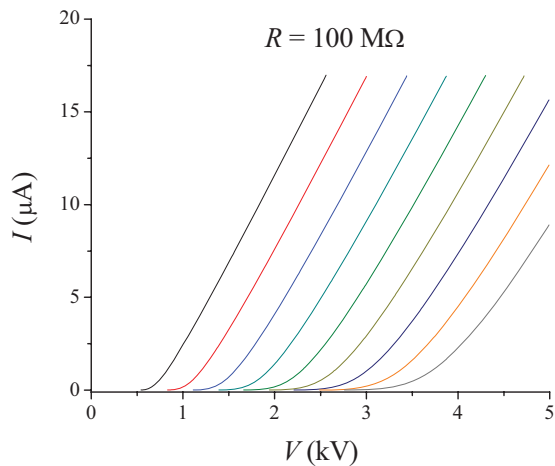
FIG. 18. (Color online) $I \times V$ behavior in a sample with high Ohmic resistance. The curves tend to straight lines for high voltages, which are not observed experimentally.

4. Radial dependence of emission

The last model we considered for a uniform distribution of emitters is a nonhomogeneous emission, i.e., the emitters are less efficient close to the z-axis than for larger r coordinate. This model is physically plausible because high current densities may cause damage to the emitters, which is common in carbon nanotubes.[24] Before any measurement, it is usual to apply a ramp voltage repeatedly. This conditioning might damage the emitters for small d where the current density is high close to the z-axis. We have two main qualitative arguments against this model and one quantitative. First, the current density is too small to cause damage to the emitters, as discussed above. Second, in copper, emission at high current density causes protrusions, which enhance the emission close to the axis.[25] This should cause a concave up in $V(d)$, which is contrary to what was observed. Despite these reasons, even if we impose a nonhomogeneous emission with bad emitters close to the axis, the fitting with the experimental data is unreasonable. If the damage is caused by the current density during conditioning, we expect the profile of β to coincide with this current density profile. However, to fit the experimental data, β profile must be much wider than the current density profile.

[1]C. A. Spindt, J. Appl. Phys. **39**, 3504 (1968).
[2]N. S. Xu and S. E. Huq, Mater. Sci. Eng. R **48**, 47 (2005).
[3]A. Wei, X. W. Sun, C. X. Xu, and Z. L. Dong, Appl. Phys. Lett. **88**, 2131102 (2006).
[4]Y. Gotoh *et al.*, J. Appl. Phys. **95**, 1537 (2004).
[5]V. P. Mammana, O. R. Monteiro, and L. R. C. Fonseca, J. Vac. Sci. Technol. B **22**, 715 (2004).
[6]W. B. Choi *et al.*, Appl. Phys. Lett. **75**, 3129 (1999).
[7]O. Gröning, O. M. Küttel, C. Emmenegger, P. Gröning, and L. Schlapbach, J. Vac. Sci. Technol. B **18**, 665 (2000).
[8]J. C. Maxwell, *A Treatise in Electricity and Magnetism*, 3rd ed. (Dover, New York, 1958), Vol. 1.
[9]W. R. Smythe, *Static and Dynamic Electricity*, 2nd ed. (McGraw-Hill, New York, 1950).
[10]J. D. Jackson, *Classical Electrodynamics*, 3rd ed. (Wiley, New York, 1998).
[11]J. H. Cloete and J. van der Merwe, IEEE Trans. Educ. **41**, 141 (1998).
[12]L. A. Butler, Aust. J. Phys. **20**, 117 (1966).
[13]H. C. Miller, J. Appl. Phys. **38**, 4501 (1967).
[14]R. G. Forbes, C. J. Edgcombe, and U. Valdrè, Ultramicroscopy **95**, 57 (2003).
[15]A. J. le Fèbre, L. Abelmann, and J. C. Lodder, J. Vac. Sci. Technol. B **26**, 724 (2008).
[16]R. H. Fowler and L. Nordheim, Proc. R. Soc. London, Ser. A **119**, 173 (1928).
[17]D. Nicolaescu, J. Vac. Sci. Technol. B **11**, 392 (1993).
[18]D. R. Lide, *Handbook of Chemistry and Physics*, 84th ed. (CRC, Boca Raton, FL,2004).
[19]V. Nemanic, M. Zumer, and B. Zajec, Ultramicroscopy **108**, 69 (2008).
[20]J. W. Gadzuk and E. W. Plummer, Rev. Mod. Phys. **45**, 487 (1973).
[21]Z. Liu and J. Ximen, Technical Digest of IVMC, 1997 (unpublished), Vol. 97, p. 353.
[22]J. P. Barbour, W. W. Dolan, J. K. Trolan, E. E. Martin, and W. P. Dyke, Phys. Rev. **92**, 45 (1953).
[23]Z. Chen, Q. Zhang, B. Zhu, D. den Engelsen, P. K. Bachmann, and A. Lewalter, J. Soc. Inf. Disp. **16**, 645 (2008).
[24]D. H. Kim, H. S. Yang, H. D. Kang, and H. R. Lee, Chem. Phys. Lett. **368**, 439 (2003).
[25]R. V. Latham and E. Braun, J. Phys. D: Appl. Phys. **1**, 1731 (1968).